Sensors & Transducers, Vol. 233, Issue 5, May 2019, pp. 27-32

www.sensorsportal.com

Sensors & Transducers

Published by IFSA Publishing, S. L., 2019
http://www.sensorsportal.com

Continuous Wave Single-longitudinal-mode 1342 nm Lasers: Modelling and Experiments

[1, 2] Yuanji Li, [1] Dandan Nie, [1] Hao Zhao, [1, 2] Jinxia Feng, [1, 2, *] Kuanshou Zhang

[1] State Key Laboratory of Quantum Optics and Quantum Optics Devices, Institute of Opto-Electronics, Shanxi University, Taiyuan 030006, P. R. China
[2] Collaborative Innovation Centre of Extreme Optics, Shanxi University, Taiyuan, Shanxi 030006, P. R. China
[1] Tel.: 86-351-7010554, fax: 86-351-7010500
[*] E-mail: kuanshou@sxu.edu.cn

Received: 30 March 2019 /Accepted: 30 April 2019 /Published: 31 May 2019

Abstract: A model suitable to the continuous wave single longitudinal mode1342 nm solid state laser with energy transfer upconversion and excited state absorption taken into account is established. The critical condition for robust mode hop free operation and the methods for power scaling are proposed via iteration method. The theory agrees well with the experiment.

Keywords: Single longitudinal mode, Mode hop free, Energy transfer upconversion, Excited state absorption, Temperature distribution.

1. Introduction

Continuous wave (cw) single frequency 1342 nm lasers with high output power have received great attentions due to their excellent properties of low noise, low dispersion in optical fiber and good beam quality. Using this kind of low noise light source, one can demonstrate quantum information investigations via optical fiber [1] and fabricate high power single frequency 671 nm lasers, which have found applications in optical cooling, lithium atom interferometers [2] and lithium isotope separation. To date, a few theoretical investigations about the influence of ETU or ESA on the 1342 nm laser were reported [3-5], but a self-consistent theoretical model taking into account the interactions between temperature rising, energy transfer upconversion (ETU) and excited state absorption (ESA) effects is still waiting for a detail study to precisely simulate the gain-loss relation and the output performance when the 1342 nm laser is operating in single-longitudinal-mode (SLM). In this paper, the heat deposition inside the laser gain medium due to the ETU and ESA effects were analyzed in detail, then the influence of ETU and ESA on the laser mode and power were investigated theoretically and experimentally by taking into account of the coupling relations among the thermal fractional loading distribution and temperature distribution inside the gain medium, the laser flux, the meta-stable level populations involved in ETU and ESA, and other temperature dependent variables.

2. Theoretical Analysis

Based on the data given in the literatures and the data obtained from a series of experimental measurements [6-14], the temperature dependences of

the Nd:YVO_4 crystal's spectral parameters were obtained by fitting the data as polynomials, as shown in Eqs. (1-9).

$$n_e = 2.15478 + 0.72*10^{-5}*(T-296) + 0.309*10^{-8}*(T-296)^2, \quad (1)$$

$$\alpha = 3.88*10^{-4}*T + 1.408\ (\mathrm{cm}^{-1}), \quad (2)$$

$$\sigma_e(T) = 10.3675\times10^{-19}\left(\mathrm{cm}^2\right) - 1.95\times10^{-21}\left(\mathrm{cm}^2/\mathrm{K}\right)\times T, \quad (3)$$

$$\sigma_{esa}^{l}(T) = 0.6786\times10^{-19}\left(\mathrm{cm}^2\right) - 0.095\times10^{-21}\left(\mathrm{cm}^2/\mathrm{K}\right)\times T, \quad (4)$$

$$\tau(T) = \frac{1+\exp(-25.9156/T)}{\frac{1}{90.3}+\frac{\exp(-25.9156/T)}{107.1}}\ (\mu\mathrm{s}), \quad (5)$$

$$\gamma(T) = [3.054\times\exp(0.02156\times T) + 217.63]\times10^{-19}\left(\mathrm{cm}^3/\mathrm{s}\right), \quad (6)$$

$$\alpha_T = \left(-0.6079+0.009*T\right)*10^{-6}\ \left(\mathrm{K}^{-1}\right), \quad (7)$$

$$K_c = K_{c,g}\frac{T_g}{T}, \quad (8)$$

$$K_a = K_{a,g}\frac{T_g}{T}, \quad (9)$$

where n_e, α, σ_e, σ^l_{esa}, γ, τ, α_T are the refractive index, the absorption coefficient at the pump wavelength λ_p, the stimulated emission cross-section at the laser wavelength λ_l, the ESA cross-section at λ_l, the ETU parameter, the fluorescence lifetime of the meta stable level and the thermal expansion coefficient, respectively. K_c and K_a are the thermal conductivities along the *c*-axis and *a*-axis of laser crystal, $K_{c,g}$ and $K_{a,g}$ are the thermal conductivities along the *c*-axis and *a*-axis of the laser crystal at a given temperature T_g. When the laser is operating stably in SLM, the temperature distribution inside the gain medium $T(x,y,z)$ obeys the heat conduction equations:

$$K_c\frac{\partial^2T(x,y,z)}{\partial x^2} + K_a\frac{\partial^2T(x,y,z)}{\partial y^2} + K_a\frac{\partial^2T(x,y,z)}{\partial z^2} = -\xi P_{in}\eta_\alpha r_p(x,y,z), \quad (10)$$

$$K_a\left.\frac{\partial T}{\partial z}\right|_{z=0} = H\left[T(z=0)-T_a\right],$$
$$-K_a\left.\frac{\partial T}{\partial z}\right|_{z=l_0} = H\left[T(z=l_0)-T_a\right], \quad (11)$$
$$T(x=0,A_x) = T(y=0,A_y) = T_b,$$

where ξ, P_{in}, η_α=1−exp(−αl), l, $r_p(x,y,z)$ and H are the fractional thermal loading, the incident pump power, the pump absorption efficiency of the gain medium, the length of the gain medium, the spatial intensity distribution of the pump beam, and the heat transfer coefficient between crystal and air, respectively. T_a and T_b are the temperatures of air and the heatsink, respectively. For simplicity, $r_p(x,y,z)$ is assumed to be in Gaussian distribution with a focused beam spot radius of ω_{pa} in our simulations.

If ξ is a constant independent on the temperature distribution inside the gain medium, $T(x,y,z)$ can be immediately calculated by a finite difference method and an iterative procedure considering the temperature dependences shown in Eqs.(1-9). However, due to the existence of ETU and ESA, ξ is a variable that is related to $T(x,y,z)$ via the following equations:

$$\xi = \xi_0 + \frac{\lambda_p}{\lambda_l}\frac{N_{etu}+N_{esa}}{N_0}, \quad (12)$$

$$N_{etu} = \tau\gamma\int_{Crystal} n(x,y,z)^2\,dV, \quad (13)$$

$$N_{esa} = \frac{c\tau}{n_e}\sigma^l_{esa}\Phi * \int_{Crystal} n(x,y,z)\phi_0(x,y,z)dV, \quad (14)$$

where ξ_0 is the fractional thermal loading related to the quantum defect, N_0= $P_{in}\eta_\alpha\tau\lambda_p/hc$ is the population in the upper laser level without the ETU and ESA effects, N_{etu} and N_{esa} represent the populations in the upper laser level involved in ETU or ESA effect, respectively. h and c are the Planck constant and light speed in vacuum. $\phi_0(x,y,z)$ is the normalized spatial distribution of laser photons and is assumed to be in Gaussian distribution with a beam waist of ω_l. $n(x,y,z)$ and Φ are the upper-state population density and the laser flux that can be resolved from the rate equations as following:

$$n(x,y,z) = 2P_{in}\eta_\alpha r_p(x,y,z)\lambda_p \Bigg/ \left\{\begin{array}{l} hc\left[\frac{c}{n_e}\sigma_e\Phi\phi_0(x,y,z)+\frac{1}{\tau}\right] \\ +hc\sqrt{\left[\frac{c}{n_e}\sigma_e\Phi\phi_0(x,y,z)+\frac{1}{\tau}\right]^2 + 4\gamma P_{in}\eta_\alpha\lambda_p r_p(x,y,z)/hc} \end{array}\right\}, \quad (15)$$

$$\Phi = \frac{2l_{eff}P_{out}\lambda_l}{-\ln(1-T_{oc})hc^2}, \quad (16)$$

where l_{eff} is the optical length of laser cavity, T_{oc} is the transmission of output coupler. Then the "real" temperature distribution inside the gain medium and the "real" N_{etu} and N_{esa} can be determined using Eqs. (1-16) and the iteration method introduced in [13].

Fig. 1 shows the simulated temperature distributions at x=y=1.5 mm in the laser crystal with the effects of ETU and ESA taken into account. It can be seen, the simulated temperature distribution comes to be converged after carrying out14 iterations. And the peak temperature inside the gain medium is 29 K higher than the simulation result without iterations. Fig. 2 shows the simulated thermal fractional loading distribution inside the gain medium under 60 W dual-end pumping after the "real" temperature distribution being evaluated and used to assign the temperature dependent parameter values. It can be seen that the heat deposition along the z direction (the thickness of the gain medium) is relatively uniform owing to the dual end pumping scheme.

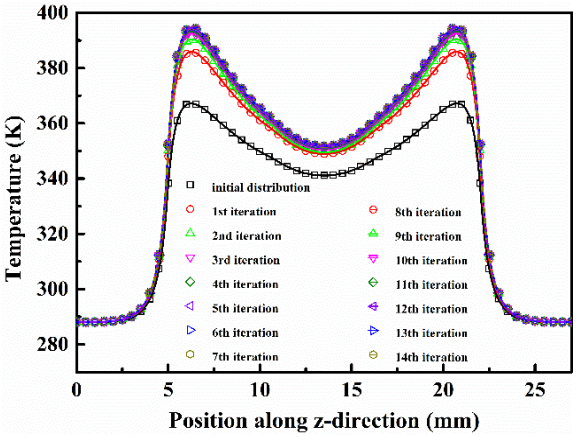

Fig. 1. Simulated temperature distribution inside the gain medium.

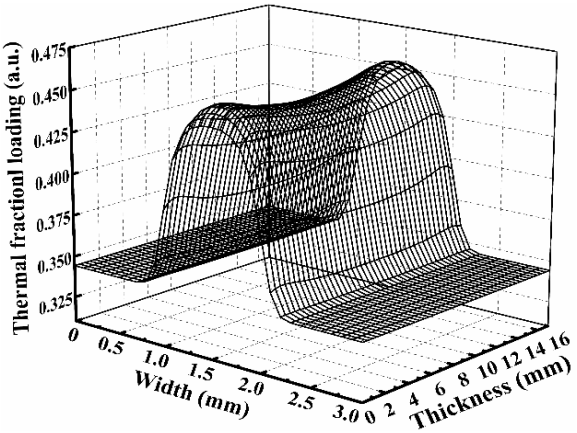

Fig. 2. Simulated thermal fractional loading distribution inside the gain medium.

Beside the thermal characteristics, the laser oscillation mode is another issues that we interested in. Since the variation of laser oscillation mode will make the frequency and power stabilities worse simultaneously, the multi-longitudinal-mode (MLM) oscillation and mode hop should be suppressed firstly by controlling the nonlinear loss and optimizing the output transmission. Based on our previous investigation [15], the sufficient condition of mode-hop-free SLM oscillation for a 1342 nm laser can be given by an inequality:

$$\frac{AK(I^2(\omega_0)+I_0 I(\omega_0))}{B(I(\omega_0)+CI_0)} > g_0^{max} l_0, \tag{17}$$

The physical basis of Eq. (17) is that when a nonlinear crystal is not inserted into the ring laser cavity and the incident pump power is high, the center mode with the frequency of ω_0 and the neighboring 2 m longitudinal modes at frequencies of $\omega_q = \omega_0 \pm q\Delta\omega$ (q=1, 2, … , m) can be oscillated simultaneously, where $\Delta\omega$ is the longitudinal-mode-spacing of the laser. In this case, all the modes experience the same losses, and the difference of gain between the center mode ω_0 and mode ω_m determined a critical net gain difference ΔG. It can be deduced that once the net gain difference between the mode ω_0 and any other mode ω_t was larger than ΔG, the oscillation of mode ω_t can be suppressed. When a dual wavelength laser is built by inserting a nonlinear crystal into the ring laser cavity, the processes of SHG and sum frequency generation (SFG) will introduce different nonlinear losses to the mode ω_0 and other neighboring modes. We could adjust the nonlinear conversion coefficient of SHG (K) to an appropriate value, in which case two following conditions can be fulfilled simultaneously. One condition is that the difference of net gain between mode ω_0 and its adjacent mode ω_1 is larger than ΔG owing to the frequency dependent nonlinear loss, and another condition is that the net gain of mode ω_0 reached the threshold condition. Eq. (17) is the mathematical expression of the two conditions, and the parameter A relates to the nonlinear conversion coefficients of SFG that is given by:

$$A = 2\mathrm{sinc}^2\left(1.39\frac{\Delta\omega}{\Delta\omega_{NL}}\right) - 1, \tag{18}$$

where $\Delta\omega_{NL}$ is the nonlinear spectral bandwidth of the nonlinear crystal. The other two parameters B and C, which are related to the number of modes located inside the gain bandwith of the gain medium can be written as:

$$B = \frac{1}{1+\frac{1}{4m^2}\left(\frac{\Delta\omega_g}{\Delta\omega}\right)^2}, \tag{19}$$

$$C = \frac{1-m^{-2}}{1+4(\frac{\Delta\omega}{\Delta\omega_g})^2}, \tag{20}$$

where $\Delta\omega_g$ is the gain bandwidth of the gain medium.

$g_0^{max} l$ is the small signal gain at the center frequency and can be represented by:

$$g_0^{max} l = \int_0^{l_0} \sqrt{1 + \frac{4\gamma\tau^2 \lambda_p P_{in} \alpha \exp(-\alpha z)}{hc\pi\omega_{pa}^2}} dz \\ * \frac{\sigma_e}{2\gamma\tau} - \frac{\sigma_e l}{2\gamma\tau}, \quad (21)$$

$I_0 = hc/(\lambda_l \sigma_e \tau_0)$ is the saturated intensity of mode ω_0, where $h\nu_l$ is the energy of laser photon. $I(\omega_0)$ is the intensity of oscillating mode ω_0 that can be written as:

$$I(\omega_0) = \begin{bmatrix} \sqrt{(\delta_0 + T_{oc} - K_0 I_0)^2 + 4K_0 I_0 g_0^{max} l_0} \\ -(\delta_0 + T_{oc} + K_0 I_0) \end{bmatrix} / (2K_0), \quad (22)$$

where δ_0 is the roundtrip dissipative loss, K_0 is the maximum value of K achieved at perfect phase matching.

The critical value of K as a function of T_{oc} for the sufficient condition of stable single frequency operation is calculated using Eqs. (1-22) and the following parameters: λ_p=880 nm, λ_l=1342 nm, P_{in}=60 W, l=18 mm, l_{eff}=190 mm, ω_{pa}=500 μm, δ_0=0.044, $\Delta\omega_{NL}$=125.7 GHz [16], $\Delta\omega_g$=255 GHz [16], $\Delta\omega$=564 MHz, T_a=298 K, T_b=288 K, A_x=A_y=3 mm, H=10 W/m^{2}K and m=6, as shown in Fig. 3. When K is located in the region above the curves, the laser can stably operate in SLM state, otherwise MLM will oscillate. It can be seen, when the output transmission is varied from 1 % to 18 %, the critical value of K is changed from 1.22×10^{-12} m^2/W to 6.58×10^{-12} m^2/W, which is always below the value of K_0 (6.7×10^{-10} m^2/W). The red and black curves in Fig. 3 (curve b and curve c) are the critical values of K versus T_{oc} with and without ETU, respectively. Comparing with the case that ETU are not considered, at a given T_{oc}, larger value of K is required to ensure stable SLM operation when ETU are taken into account.

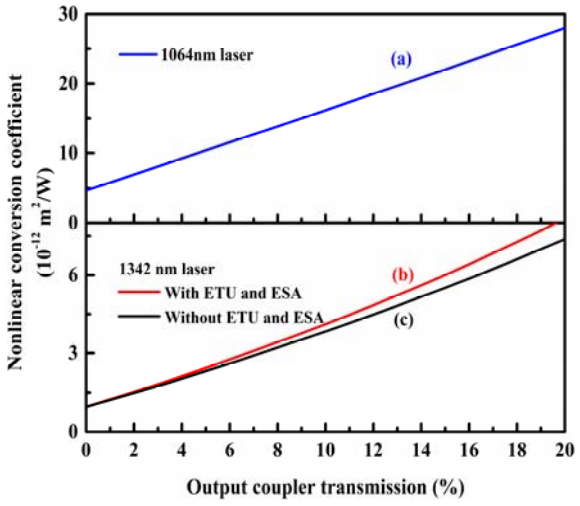

Fig. 3. The critical nonlinear conversion coefficient vs. output transmission.

3. Experimental Setup

The experimental setup of cw SLM 1342 nm laser is shown in Fig. 4. The 18 mm long wedged Nd:YVO_4 crystal is dual-end pumped by polarized 880 nm lasers provided by a laser diode and the pump spot radius inside the gain medium is 500 μm. For longitudinal mode selection, a 190 mm-long ring resonator composed of 6 mirrors and an optical diode is employed. A type-I noncritical phase-matched LBO crystal is inserted into the ring laser cavity for introducing nonlinear loss. The 1342 nm laser from the resonator is split into three parts, and the characterization of the laser is demonstrated by a power meter (PM_1), a Fabre-Perot (F-P) interferometer ($F\text{-}P_2$) and a balanced detection system (BD). A stabilization system based on $F\text{-}P_2$ interferometer is also employed to suppress the frequency fluctuation.

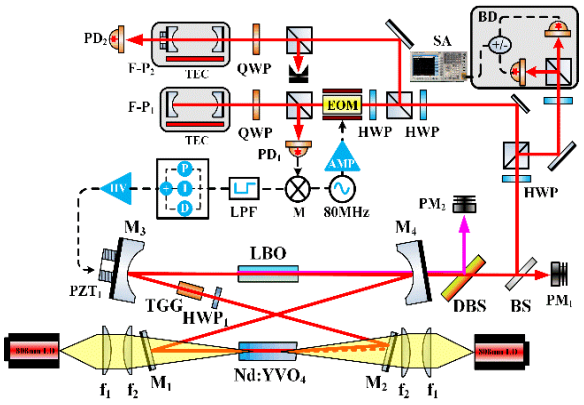

Fig. 4. Experimental setup of cw SLM 1342 nm laser.

4. Experimental Results and Discussions

Fig. 5 shows the dependences of the 1.34 μm laser output on transmission of output coupler at a boundary temperature of 288 K and an incident pump power of 60 W under dual-end pumping. The circles are experimental data. The red curve is the theoretical prediction considering both ETU and ESA effects that are in good agreement with experimental results. As a comparison, the black curve is the theoretical prediction without both ETU and ESA effects that deviate significantly from experimental results. The blue curve is the theoretical prediction without only ESA effects that has the same tendency with the red curve, but lower at higher output transmission. It can be seen, there exists an optimum output transmission to achieve a maximum laser output. When ETU and ESA effects are considered the optimum transmission of output coupler is 7.2 %, but in the cases that the two effect or only the ETU was neglected, it should be 5.8 % and 10 %, respectively. Moreover, when the total pump power was 60 W and the output coupler with a transmission of 10 % was employed, 16.2 W cw SLM 1342 nm laser operation was experimentally realized.

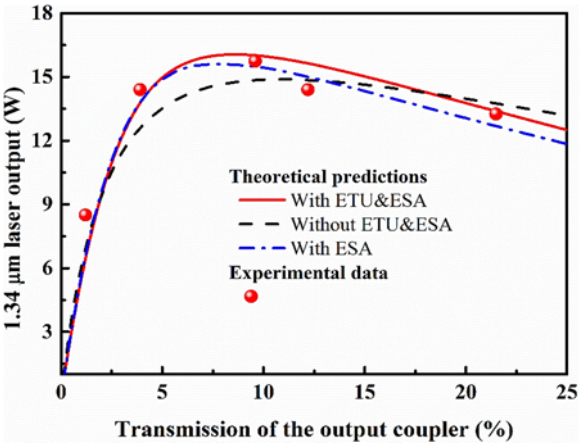

Fig. 5. Output power of cw SLM 1342 nm laser as a function of the output tramission.

Figs. 6-8 show the laser mode structure under 60 W pumping, the frequency fluctuation before and after laser frequency stabilization and the intensity noise properties of the 1342 nm laser. It can be seen, using an F-P cavity frequency reference, the SLM mode hop free laser operation is confirmed. Moreover, the frequency fluctuation of the free running 1342 nm laser was ±3.1 MHz in a given 5 hours, once the frequency stabilization loop was working, the laser frequency fluctuation was suppressed to ±0.2 MHz in a given 3 hours. The laser intensity noise reached the shot noise limit beyond the analysis frequency of 3 MHz.

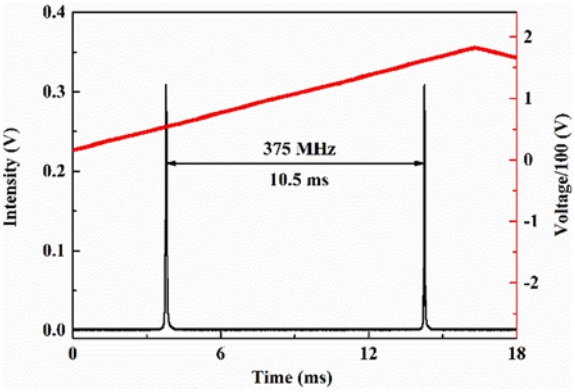

Fig. 6. Frequency behaviors of 1342 nm laser.

5. Conclusions

We demonstrate the modelling and experimental fabrication of a cw single frequency 1342 nm solid state laser. The model is self-consistent by taking into account the coupling relations among the thermal fractional loading distribution and temperature distribution inside the gain medium, the laser flux, the meta-stable level populations involved in ETU and ESA, and other temperature dependent variables via an iteration method. A 16.2 W cw single frequency 1342 nm laser source with no mode hop, ±0.2 MHz long term frequency stability, and shot noise limit intensity noise performance beyond 3 MHz is built. The theoretical prediction is in good agreement with the experimental results.

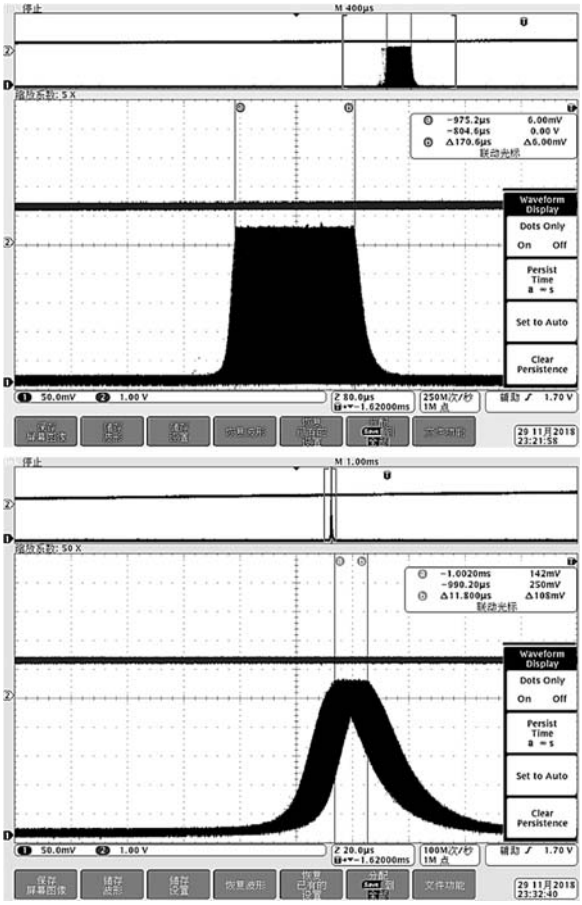

Fig. 7. Frequency fluctuations of 1342 nm laser.

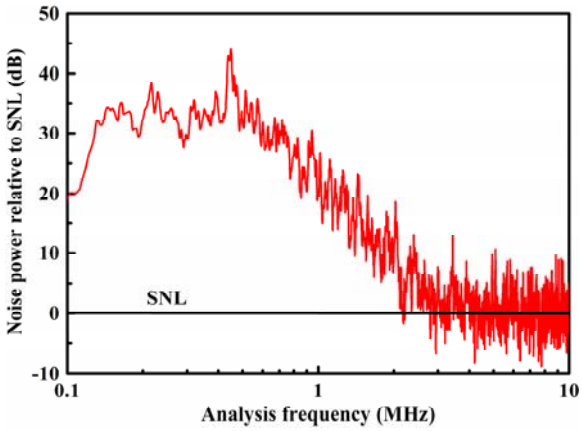

Fig. 8. Intensity noise of 1342 nm laser.

Acknowledgements

This work was supported by the National Key R&D Program of China (2017YFB0405203).

References

[1]. M. R. Huo, J. L. Qin, J. L. Cheng, Z. H. Yan, Z. Z. Qin, X. L. Su, X. J. Jia, C. D. Xie, K. C. Peng, Deterministic quantum teleportation through fiber channels, *Science Advance*, Vol. 4, Issue 10, 2018, eaas9401.

[2]. N. Kretzschmar, U. Eismann, F. Sievers, F. Chevy, C. Salomon, 2.4-watts second-harmonic generation in ppZnO:LN ridge waveguide for lithium laser cooling, *Optics Express*, Vol. 25, Issue 13, 2017, pp. 14840-14855.

[3]. M. Okida, M. Itoh, T. Yatagai, H. Ogilvy, J. Piper, T. Omatsu, Heat generation in Nd doped vanadate crystals with 1.34 μm laser action, *Optics Express*, Vol. 13, Issue 13, 2005, pp. 4909-4915.

[4]. Y. F. Chen, L. J. Lee, T. M. Huang, C. L. Wang, Study of high-power diode-end-pumped Nd:YVO_4 laser at 1.34 μm: influence of Auger upconversion, *Optics Communication*, Vol. 163, Issue 4-6, 1999, pp. 198-202.

[5]. Y. H. Zheng, Y. J. Wang, C. D. Xie, K. C. Peng, Single-frequency Nd:YVO_4 laser at 671 nm with high-output power of 2.8 W, *IEEE Journal of Quantum Electronics*, Vol. 48, Issue 1, 2012, pp. 67-72.

[6]. Y. J. Wang, W. H. Yang, H. J. Zhou, M. R. Huo, Y. H. Zheng, Temperature dependence of the fractional thermal load of Nd:YVO_4 at 1064 nm lasing and its influence on laser performance, *Optics Express*, Vol. 21, Issue 14, 2013, pp. 18068-18078.

[7]. N. Ter-Gabrielyan, V. Fromzel, M. Dubinskii, Linear thermal expansion and thermo-optic coefficients of YVO_4 crystals the 80-320 K temperature range, *Optical Materials Express*, Vol. 2, Issue 11, 2012, pp. 1624-1631.

[8]. D. E. Zelmon, J. J. Lee, K. M. Currin, J. M. Northridge, D. Perlov, Revisiting the optical properties of Nd doped yttrium orthovanadate, *Applied Optics*, Vol. 49, Issue 4, 2010, pp. 644-647.

[9]. G. Turri, H. P. Jenssen, F. Cornacchia, M. Tonelli, M. Bass, Temperature-dependent stimulated emission cross section in Nd^{3+}:YVO_4 crystals, *Journal of the Optical Society of America B*, Vol. 26, Issue 11, 2009, pp. 2084-2088.

[10]. Y. G. Zhao, H. H. Yu, Z. P Wang, H. J. Zhang, X. G. Xu, J. Y. Wang, Homogeneous and inhomogeneous spectrum broadening in Nd^{3+}-doped mixed vanadate crystals, *Optical Materials*, Vol. 71, 2017, pp. 78-85.

[11]. N. A. Tolstik, G. Huber, V. V. Maltsev, N. I. Leonyuk, N. V. Kuleshov, Excited state absorption, energy levels, and thermal conductivity of Er^{3+}:YAB, *Applied Physics B*, Vol. 92, Issue 4, 2008, pp. 567-571.

[12]. M. Laroche, S. Girard, J. K. Sahu, W. A. Clarkson, J. Nilsson, Accurate efficiency evaluation of energy-transfer processes in phosphosilicate Er^{3+}-Yb^{3+}-codoped fibers, *Journal of the Optical Society of America B*, Vol. 23, Issue 2, 2006, pp. 195-202.

[13]. Y. Y. Ma, Y. J. Li, J. X. Feng, K. S. Zhang, Influence of energy-transfer upconversion and excited-state absorption on high power Nd:YVO_4 laser at 1.34 μm, *Optics Express*, Vol. 26, Issue 9, 2018, pp. 12106-12120.

[14]. Y. J. Li, D. D. Nie, H, Zhao, J. X. Feng, K. S. Zhang, Power scaling and mode-hop suppression of continuous wave single-longitudinal-mode 1342 nm lasers, in *Proceedings of the 2nd International Conference on Optics, Photonics and Lasers (OPAL' 2019)*, Amsterdam, The Netherlands, 24-26 April 2019, .pp. 56-58.

[15]. Y. Y. Ma, Y. J. Li, J. X. Feng, K. S. Zhang, High-power stable continuous-wave single-longitudinal-mode Nd:YVO_4 laser at 1342 nm, *Optics Express*, Vol. 26, Issue 2, 2018, pp. 1538-1546.

[16]. H. D. Lu, J. Su, Y. H. Zheng, K. C. Peng, Physical conditions of single-longitudinal-mode operation for high-power all-solid-state lasers, *Optics Letters*, Vol. 39, Issue 5, 2014, pp. 1117-1120.